DOI: 10.1002/adma.((please add manuscript number))

# Ecologically driven ultrastructural and hydrodynamic designs in stomatopod cuticles

By *L.K. Grunenfelder, G. Milliron, S. Herrera, I. Gallana, N. Yaraghi, N.C. Hughes, K. Evans-Ludderodt, P. Zavattieri, D. Kisailus**

[*] Dr. Lessa Kay Grunenfelder, Dr. Garrett Milliron, Steven Herrera, Nicholas Yaraghi, Prof. David Kisailus (corresponding author)

Department of Chemical and Environmental Engineering, Materials Science and Engineering Bldg. Room 343, UC Riverside, Riverside, CA, 92521, USA
E-mail: david@engr.ucr.edu

Prof. Nigel Hughes

Department of Earth Sciences, UC Riverside, Riverside, CA, 92521, USA

Isaias Gallana,

Lyles School of Civil Engineering, Purdue University, West Lafayette, IN, 47907, USA

Departamento de Aeronautica, Universidad Nacional de La Plata, Argentina

Prof. Pablo Zavattieri
Lyles School of Civil Engineering, Purdue University, West Lafayette, IN, 47907, USA

Kenneth Evans-Ludderodt

National Synchrotron Light Source, Brookhaven National Laboratory, Upton, NY 11973, USA

Keywords: (Composites, Toughness, Impact, Biomineral, Ultrastructure)

Ecological pressures and varied feeding behaviors in a multitude of organisms have necessitated the drive for adaptation. One such change is seen in the feeding appendages of the stomatopods, a group of highly predatory marine crustaceans. Stomatopods include "spearers," who snare soft bodied prey using an ambush style attack, and "smashers," who bludgeon hard shelled prey with a heavily mineralized club. The regional substructural complexity of the stomatopod dactyl club from the smashing predator *Odontodactylus scyllarus* represents a model system in the study of impact tolerant biominerals. The club is a multi-regional composite, consisting of a highly mineralized impact region, a characteristic Bouligand architecture (which is common to arthropods), and a unique section of the club, the striated region, composed of highly aligned sheets of mineralized fibers. A detailed ultrastructural investigation of the striated region within *O. scyllarus* and a related species of spearing stomatopod, *Lysiosquillina maculate* shows a consistent organization of mineral and organic, but distinct differences in the macro-scale architecture of the region across species. Evidence is provided for the function and substructural exaptation of the striated region, which facilitated redeployment of a raptorial feeding appendage as a biological hammer. Moreover, given the need to accelerate underwater and "grab" or "smash" their prey, the spearer and smasher appendages are specifically designed with a significantly reduced drag force. Interestingly, advanced engineering structures, including aerodynamic bicycle helmets and golf clubs, incorporate similar structural designs suggesting that Nature's evolutionary progression has inadvertently used internal modeling processes via adaptation to achieve its own high performance structures.

**Introduction**

Stomatopods, commonly referred to as mantis shrimp, are aggressive Crustacea known for their raptorial predatory strike, which exemplifies one of the fastest known animal movements [1]. In general terms, stomatopods can be divided into two groups: the "spearers" that attack soft-bodied prey with a harpoon-like structure, and the more recently evolved "smashers" that crush hard-shelled prey using a hammer-like club. [1-3] The stomatopod fossil record, which extends back at least 350 million years (MA), [4] suggests that early stomatopods employed multiple raptorial, thoracic appendages in prey capture using spearing action. However, some 150 MA ago the second thoracic appendage became distinctly prominent.[5,6] In many living groups this appendage retains spearing function, but characters associated with the smashing habit evolved by 70 MA.[7,8] Recent phylogenetic analyses based both on form [9] and genes [10] are congruent in suggesting smashing to be a derived habit. The appearance of the earliest smashers contributed to a dramatic rise in the number of marine families employing predation by shell breakage that was part of the Mesozoic marine revolution.[11,12] This evolutionary diversification was accompanied by an "arms race" between predators with increasingly sophisticated weaponry and prey with more effective defenses. The appearance of the stomatopod smashing habit coincided both with the appearance of several new clades of fish, other kinds of crustaceans, and predatory gastropods[11] that target shell dwellers specifically. Patterns of shell damage arguably specific to smashing stomatopods are known among fossils and extend back at least 15 MA.[13,14]

*Odontodactylus scyllarus* (Figure 1A) is a smashing stomatopod, which employs a raptorial strike that reaches speeds of 14-23 m/s.[15] *Lysiosquillina maculate* (Figure 1B), in

contrast, is a member of the evolutionarily older group of spearing species.[2] Spearing stomatopods utilize a slower strike (average linear speed 2.3 m/s) in an ambush-style attack.[16] While spearing stomatopods exhibit an elongated and barbed raptorial appendage, smashing stomatopods possess a bulbous dactyl club.

Past investigations into the ultrastructure and impact tolerance of the smashing dactyl club from *Odontodactylus scyllarus* revealed, via observations of a transverse cross-section of the club, a multi-regional structure consisting of impact, periodic, and striated regions.[17] The impact region is homologous to the exocuticle of arthropods, while the periodic and striated regions constitute the endocuticle. The periodic region is named for its optically visible periodicity, which results from helicoidally stacked α-chitin sheets embedded in a mineral matrix. This Bouligand, or twisted plywood, structure is the established substructural architecture of arthropod cuticle.[18]

In contrast to this well-known structure, the striated region exhibits microstructural features which deviate significantly from the helicoidal motif, initially suggested to be formed from parallel bundles of mineralized rods with α-chitin cores.[17] This region is a unique feature of the stomatopod cuticle, with implications for impact resistance.[19] The aligned fibers of the striated region wrap around the circumference of the stomatopod club, in much the same way that boxers wrap their hands with tape before a fight. The role of the striated region in preventing damage from a high-energy strike has been interrogated through preliminary finite element models. The region has been shown to provide resistance against lateral deformation of the club, along with compressive and torsional stiffness.[17] The atypical architecture of the region is well suited to such a purpose, as aligned fiber composites are known to be stiff and strong in the fiber direction.[20] The strike from a spearing stomatopod is different from that of a smashing stomatopod and therefore, we pose the question: If the forces exerted are different, is

there a change in the underlying microstructures within the dactyls? To address this question, we probe the ultrastructures of the striated region in both spearing and smashing stomatopods, demonstrate the proposed function of the region with simulations and physical models, and provide retrodictive evidence for its exaptation.

**Structural characterization of the dactyl club of *O. scyllarus***

Examination of the dactyl club of *Odontodactylus scyllarus* by optical and electron microscopy reveals a complex architecture. Sectioning the club through three orthogonal planes (sagittal, coronal, and transverse, Figure 2A) provides a three-dimensional view of the ultrastructural features within the club. Optical micrographs (Figure 2B-E) provide wide field views of the bulk features of the club, with a transverse cross section (Figure 2D, E) demonstrating the multi-regional nature of the club. The striated region (dashed yellow line, Figure 2E) is observed on either side of the periodic region (which constitutes the majority of the endocuticle) and is adjacent to the exterior surface. Observations of a coronal section (Figure 2C) uncovered that the striated region wraps around the circumference of the club.

A transverse fracture (Figure 2F) of the club highlights that the region is shown to indeed be composed of stacked layers of mineralized sheets. Here, the fibers composing the sheets are oriented perpendicular to the field of view. A coronal fracture (Figure 2G) reveals the presence of pore channels running left to right (highlighted in yellow), with the mineralized fibers that make up each layer of the striated region extending from top to bottom. Pore channels run from the interior of the club outward, traversing the entire club and continuing through the periodic region (Supplemental Figure 1) and are similar in design to the pore

channel networks observed in other Crustacea including lobster [21-23] and crab.[24,25] These observed pore channels likely serve as ion transport pathways during mineralization, and potentially enable self-healing.[23] An ion polished sagittal section provides a clearer view of the geometry of pore channels (Figure 2H), which are circular in cross-section, with an average diameter of 246 ± 52 nm and constitute an area fraction of 0.53 ± 0.06 %. In typical crustacean exoskeletal regions, pore channels run perpendicular to the rotating Bouligand fiber layers, and thus take on a twisted ribbon appearance.[21,26] Because the striated region is formed from mineralized fibers oriented in one direction, however, the clearly visible pore channels in this region run straight, perpendicular to the aligned fibers.

The mineral phase in the striated region is composed primarily of amorphous calcium carbonate and calcium phosphate.[17] The details of the arrangement of the organic material within the mineral are an important factor in understanding the mechanical properties of the region, and are provided through microscopic analyses of demineralized specimens (Figure 2I), transmission electron microscopy (TEM), and synchrotron x-ray diffraction (see Supplemental Figure 3). These investigations confirm that the striated region indeed consists of aligned α-chitin fibers oriented parallel to sagittal or coronal sections, and are therefore perpendicular to a transverse section. The organic fibers that form the scaffold of the striated region likely act to template the formation of mineral, yielding a laminated structure.

The interspersed network of pore channels, along with the interfaces between mineralized fiber sheets, give the striated region its striped appearance. A fully developed three-dimensional schematic of the region is presented in Figure 2J, with the mineralized fibers layers in gray, interfaces in blue, and pore channels in yellow. A corresponding arrangement of SEM micrographs is shown in Figure 2K.

**Evolutionary adaptation: from spearer to smasher**

The forces exerted during a strike, and thus the underlying structures within the dactyls of spearing and smashing stomatopods, should be different. During an impact event, the dactyl of *O. scyllarus* folds into the adjacent propodus to form a functional club.[3,17] The organism is capable, however, of separating these two segments, revealing a spike that protrudes from the dactyl. This spike functions as a piercing weapon, used to impale soft-bodied prey.[27] Unlike the functional club utilized by the smashing stomatopods, the spearing species elongate and separate the dactyl, propodus and merus during attack, grasping prey between the dactyl and propodus.[16] How these disparate structures influence the stresses generated during a raptorial strike in spearing and smashing species remains unknown. This mystery is best resolved through examination and comparison of the ultrastructure of the smashing stomatopod with its spearing ancestor.

Low magnification electron micrographs of intact and demineralized transverse cross sections at two different positions within the smashing dactyl of *O. scyllarus* and the dactyl of the spearing species, *L. maculate* reveal (Figure 3) the highly oriented mineralized fibers within the striated region (which run perpendicular to the transverse cross section). The rapid demineralization along the fiber direction clearly distinguishes the striated region from the periodic and impact regions, which contain organic layers oriented within the transverse plane, preventing rapid demineralization.

A comparison of transverse cross-sections from the dactyl club of *O. scyllarus* (Figure 3A-C) at the center of the bulb, near the impact zone (dashed blue line) and at the basal support

of the protruding spike (dashed red line) reveals a significant change in the location of the striated region. In the region of the protruding spike (Figures 3 B, C) the striated region wraps around the entire structure, while in the bulbous region of the club, where impact occurs, the striated region takes on a different morphology (Figure 3D, E). Here, the region is observed only on the sides of a transverse cross section, indicating that it wraps the club, from the top of the bulb to the tip of the spike, but does not extend to the impact surface. This modification to the striated region results in enhanced impact resistance. Upon impact, the helicoidally oriented fiber layers in the periodic region are compressed, leading to a state of biaxial stress in the plane of each sheet. This, in turn, causes Mode I fractures to nucleate and grow within the periodic region. The nucleation, growth, and control of these fractures is the dominant energy dispersion mechanism in the club.[19] Confining cracks within the periodic region is critical to avoiding propagation of fractures through to the surface of the club, which would result in catastrophic failure. The striated region, with aligned fibers wrapping around the circumference of the club, is able to withstand the out of plane tensile loads induced by strain in the periodic region, providing support to the energy absorbing periodic region and aiding in the containment of cracks within the interior of the club. By limiting the strain within the periodic region to allow fractures nucleate and grow, while at the same time constraining their driving force, an optimal energy dispersive and impact resistant structure is formed.[28] Similar observations have been reported for unconfined and confined brittle materials under dynamic impact.[29-31] This mechanism is explored in further detail in the following section, through the implementation of finite element models.

If, as hypothesized, the striated region serves the function of preventing catastrophic propagation of cracks in the bulb of the stomatopod club during impact, a natural question arises: why does the region surround the spike of the club?

Cross sectional views near the tip (dashed yellow line, Figure 3F, G, H) and the center (dashed green line, Figure 3F, I, J) of a dactyl spear from *L. maculate* reveal a striated region that wraps around the entire structure at the tip (Figure 3 G, H). This is in contrast to the morphology observed in the club of *L. maculate*, which nearly connects in the location analogous to the impact surface of a smasher, at the center of the spear (Figure 3 I, J). Unlike the club of the smasher, the critical loading condition encountered by a spearing dactyl is not directional impact loading, but rather a multi-directional flexural stress. A striated region, with aligned fibers oriented along the long axis, is an ideal substructure to support the torsional loading of a high aspect-ratio spear. In fact, because the perimeter of beam's cross-section experiences the largest stresses when loaded, it is common practice in the design of composite materials to reinforce a flexural member with longitudinal fibers.[32,33] Despite significant differences in the macrostructure between spearing and smashing stomatopods, fractured surfaces of both dactyls confirm that the striated regions have similar microstructures (see Supplemental Figures 3 and 4). This aligned, fiber-reinforced design of the striated region has been adapted from spearing stomatopods into the club of smashing species.

**The mechanical role of an evolving striated region**

Understanding the role of the striated region within the dactyls requires first understanding stresses within the primary energy-absorbing region (i.e., the Periodic region). Previous observations have reported that microcracks tend to follow the motif of the helicoidal pattern inside the periodic region.[17] The fact that cracks grow between fibers may be an indication that the interfacial strength between fibers is somehow inferior compared with the tensile strength of the fibers. To investigate the role of the spatial distribution of stress within

the periodic region, and infer how that affects the damage mechanisms, we analyzed a series of striking events against a solid target using dynamic finite element modeling (DFEM) (Figure 4A). It was revealed that a large portion of the center of the period region is predominantly under tensile stress in the plane of the fibers (i.e., perpendicular to the z-axis in Figure 4B), while under compressive stresses in the *z*-direction. In particular, we highlight in dark blue regions where the in-plane tensile stress is mostly biaxial (i.e., the radial stress, $\sigma_r$, has a similar magnitude as the hoop stress, $\sigma_\theta$). This indicates that interfaces between fibers are mostly in opening (mode I) load and cracks can propagate in the z-direction following a twisted pattern (See inset of Figure 4B). The implications are that even if the crack front twists, the dominant crack propagation driving force is still mode I. This may result in the nucleation of multiple cracks and twisting crack growth along the z-direction, which results in nested patterns. Such patterns were confirmed by experimental observations reported in previous work.[17,19] We surmise that this strategy maximizes the crack area per unit volume and therefore the energy dissipation capacity of the periodic region without the creation of dominant and localized cracks that may lead to catastrophic failure of the dactyl club.

The extent to which the internal stresses can produce sufficient damage depends on the impact velocity and peak loads produced during the impact event. However, high values of stress may be counteracted by lateral confinement provided by the striated region to prevent the in-plane tensile stresses from reaching critically high values. Further examination of the maximum principal stress indicates that the $\alpha$-chitin fibers are in tension during the dynamic impact event. Figure 4C shows the maximum principal stress in the striated region where the principal direction, indicated by arrows, is aligned parallel to the direction of the fibers. Thus it is likely that the fibers work as a confining "belt", preventing lateral expansion and controlling the tensile stress and damage in the center of the periodic region. Since the elastic properties of

the striated region in the transverse and coronal sections do not show significant differences, the structure has been modeled as an isotropic elastic solid. A subsequent investigation comparing different levels of stiffness in the region revealed that the tensile stress in the center of the periodic region (indicated with an x in Figure 4B) is indeed attenuated by a stiff striated region (Figure 4D). It should be noted that the measured Young's Modulus of the striated region is around 15 GPa (see Supplementary material).

As discussed, the dactyl spike in the smashing stomatopod is more than just a vestigial remnant from a spearing ancestry. The club is multifunctional, used both to impact hard-bodied prey, and to impale soft-bodied targets. The striated region, first evolved to support torsional loads in dactyl spears, performs the same function in the spike of the dactyl club. Additionally, as the spear evolved into a biological hammer, the striated region co-evolved, adapting to support impact loading and prevent catastrophic failure during a high-energy strike.

While the redeployment of the striated region was a key evolutionary consideration in the transition from spearing predation to smashing behavior, it is not surprising that other alterations occurred as well. Claverie et al. reported that each article of the stomatopod raptorial appendage (i.e., dactyl, propodus, and merus) is a unique developmental module, able to evolve independently.[34] Examination of the merus of smashing and spearing species reveals particularly prominent differences. The merus of the smashing stomatopod is noticeably larger than that of the spearing organism.[35] Additionally, key differences exist in various components of the merus (saddle and meral-V) between spearers and smashers, with implications in power amplification mechanisms.[16,36] It has also been reported that smashing stomatopods have a greater density of muscle mass in their raptorial appendages. [35] While an ambush-style spearing attack requires speed and precision, the fastest reported strikes have been observed in

smashing stomatopods, where high speeds translate into large impact forces.[16] The slower movement of the spearing stomatopod is precise, utilizing direct muscle control, while the rapid strike of the smashing species relies upon elastic energy storage in the larger, more muscular merus.[16,37] This is a topic of ongoing investigation.

From the structural point of view, the spearer spike and smasher dactyl club have to resist deformation from interaction with prey as well as the viscous forces of water during the attack. For very slender structural members such as the spearer spike, one particular concern is the ability of the appendages to remain rigid and therefore maintain effectiveness to grab and spear. Considering the variation of the cross section geometry and distribution of the elastic properties, Figure 5A shows the variation of the bending stiffness $K_{xx}$ and $K_{yy}$ along the two principal directions, $x$ and $y$, showing a compliant structure for bending around the axis $x$ and a much stiffer for bending around $y$. On average, $K_{xx}$ has a similar bending stiffness of an equivalent circular cross section with the same dimension, $d$, elastic properties and area, $K_c$. We also note that the torsional stiffness of the spike, $K_t$, is not significantly lower than that of the equivalent circular cross section area, $K_c$, as one would expect of a slender structure. This makes the spike exceptionally efficient to resist deformation when grabbing fish while still maintaining a hydrodynamic profile. A similar analysis is shown for the smasher dactyl club in Figure 5B. For this particular case, the intricate profile of the dactyl club at its center makes its bending and torsional stiffness higher than its circular cross section equivalent. We hypothesize that such high resistance to bending and torsion is necessary for when the stomatopod employs its dactyl club to spear its prey. Such a geometry also allows for additional mass to help build momentum during a strike.

The ability to resist bending and torsional deformation during the strike is also combined with the spearer spike and dactyl club characteristic hydrodynamic profile. To assess

the drag forces of these profiles, we compare the appendage profiles with geometries of known Drag coefficients, $C_d$. Considering the viscous behavior of water, typical dimensions of these appendages and the velocities reached during the strike, we estimated Reynolds ($Re$) numbers between $9x10^4$ and $4x10^6$ (both well above the limit for turbulent flow in water, $Re > 10^4$). While the spearer spike was compared with circular and elliptical profiles, the middle section of the smasher club was compared with a circular, a bullet shaped cross-section and an airfoil cross-section. A quick comparison reveals that $C_d$ of an elliptical profile that resembles the spike (4:1 in Figure 5C) is half of the circular cross section. Conversely, Figure 5D reveals that the drag coefficient of a bullet shape (that resembles the cross section of the dactyl club) does not seem to vary from that of a circular one. However, when we consider an airfoil profile that resembles the entire dactyl club/propodus functional club, $C_d$ decreases by more than one order of magnitude. This remarkable hydrodynamic property is supported by the fact that the dactyl club and propodus do not separate during the strike process. While previous work indicated that the propodus does not have a relevant role in the impact force[17], the information presented here indicates that the propodus may indeed help reduce the drag force and therefore make the strike more effective. Interestingly, the $C_d$ of an airfoil profile based on the geometry of an aerodynamic helmet used for racing bicycles is similar to that of the dactyl club/propodus geometry (See Figure 5D).

**Convergent evolution: comparison with an insect eponym**

The striated region observed in the stomatopod dactyl is a unique additional architectural feature within the crustacean cuticle, which like all arthropod exoskeletons, typically favors a Bouligand design.[19] It is conceivable, however, that a similar structure may

exist in convergently evolved organisms that also utilize a raptorial feeding strike. To investigate this possibility, the dactyl of the mantis shrimp's insect namesake, the praying mantis, was examined. The praying mantis, like the stomatopod, is an arthropod with a cuticle consisting of helicoidally arranged α-chitin fibrils.[38] To determine if the praying mantis utilizes aligned chitinous architectures analogous to the striated region in the stomatopod, a tibia (the segment corresponding to the dactyl in the stomatopod) of the praying mantis *Stagmomantis limbata* (Figure 6A) was sectioned transversely (Figure 6B). Close examination of this transverse section (Figure 6C) reveals that its structure is formed with a laminated architecture, visually similar to the periodic region of the stomatopod dactyl club. However, we do observe layers of fibers that is radially aligned to the tibia (See Supplemental Figure 5), quite similar to the striated region of the spearing mantis' dactyl (as well as the spike of the smashing mantis' dactyl). This is reasonable considering that the tibia of the praying mantis may also undergo torsional loading. However, the cross-section of the praying mantis tibia is different from that of the stomatopod dactyl, exhibiting a wide triangular shape, in contrast to the thin elliptical cross section observed in spearing stomatopods.

The differences in the praying mantis' cross-sectional profile can be explained by considering the environmental differences encountered by these otherwise similar organisms. The praying mantis is a land animal, feeding in air, a medium 3 orders of magnitude less dense than the aquatic environment of the stomatopod. The drag force encountered by the dactyl of the stomatopod is, therefore, far more limiting than the air resistance felt by the praying mantis. Because fluid resistance is proportional to the product of the density and the cross sectional area of a structure (along with the velocity of the body),[39] the thin cross-section of the spearing stomatopod's dactyl is critical to achieving fast and controlled movements underwater. The addition of a mineralized longitudinal fiber reinforcement, achieved by the evolution of a

striated region, is an optimized design to increase torsional strength while maintaining a narrow cross-section.[32] Critical to the ambush-style attack of the spearing stomatopod is a minimization of disturbance to the surrounding water.[16] A successful aquatic ambush predator must move rapidly through the water without pushing water, and therefore prey, away.[16] This is an additional benefit to the streamlined design of the spearing dactyl. The smashing stomatopod, in contrast, requires a wider cross-section to deliver damaging blows to prey, and has therefore evolved a more robust power amplification system to compensate for fluid resistance.[36,37,40] The cross-section of the praying mantis' tibia is wider than that of the spearing stomatopod, with a near zero eccentricity, leading to an isotropic section modulus.

**Conclusions**

The striated region observed in the dactyl club and spearing appendages of the stomatopod is a unique architectural element, not found in other Crustacea. The region is composed of aligned α-chitin fibers, a departure from the common helicoidal motif. In spearing stomatopods, the striated region provides support to a long, thin, raptorial spike. The region has been redeployed, however, in the evolutionarily derived smashing stomatopods, to perform not only this original function, but also to support high-energy impact loading, preventing catastrophic cracking of the structure. The incorporation of a striated region is critical to the function of rapid raptorial strikes in both aquatic and terrestrial predators that undergo torsional stresses. It is likely that the incorporation of a striated region aided in the advent of smashing predators in the stomatopod family.

The repurposing of the dactyl into a club was accompanied by alterations in the remainder of the raptorial appendage to accommodate elastic energy storage and enable the

staggering speeds and accelerations required to generate devastating blows. Considering the need to accelerate under water and "grab" its prey, the spearer spike is specifically designed for striking without sacrificing torsional and bending stiffness. Conversely, the dactyl club presents a more robust structure, yet remarkably its assault is orchestrated by the dactyl operating in tandem with the propodus to significantly reduce the drag force. Interestingly, current designs in advanced engineering structures, such as aerodynamic bicycle helmets and golf clubs, incorporate similar designs. This suggests that Nature's evolutionary progression has inadvertently used internal modeling processes via adaptation to achieve its own high performance structures.

Specialization in mineralized chitin structures for the fulfilment of specific functions has been observed across biological composites. The striated region in the stomatopod dactyl club, as detailed here, is mineralized with amorphous calcium carbonate and calcium phosphate, and specialized for impact resistance. A recent study revealed that chitin is also present in the center of *S. hawaiicus* sponge spicules, in the form of concentric chitin/silica laminated nano-layers which serve to increase flexibility and prevent demineralization of the structure under exposure to alkali environments.[54] In addition to structural benefits, the mineralized spicules in *S. hawaiicus* facilitate transmission of light through the layers, with a structure reminiscent of photonic fibers. Another classic example is the parallel lamella of chitin-templated aragonite (crystalline $CaCO_3$) pillars observed in the internal skeleton of cuttlefish (*S. officinalis*).[55] The structure of cuttlefish bone allows for resistance to external hydrostatic pressures, while the hollow aragonite pillars can be filled with varying quantities of liquid to alter the buoyancy of the organism. As these examples illustrate, chitin is a versatile template for the highly organized growth of diverse minerals in biological systems, enabling specialization across a range of functionalities.

**Experimental Section**

Specimen Handling

Live specimens of *Odontodactylus scyllarus* and *Lysiosquillina maculate* were obtained from a commercial supplier. *Odontodactylus scyllarus* were housed in individual acrylic tanks in a recirculating artificial seawater system. *Lysiosquillina maculate* were housed in a large polymer aquarium containing sand to enable the organisms to create burrows. For analysis, dactyl clubs and spears were removed, rinsed in DI water, and air-dried at room temperature.

Examination of a pore canal network in the stomatopod club

Fractured sections of stomatopod dactyls were prepared using a razor blade. Samples were sputter coated with a thin layer of platinum and palladium and imaged using a scanning electron microscope (XL30-FEG, Philips, USA) at an accelerating voltage of 10 kV.

To obtain a more detailed view of the pore canal structure, sagittal sections were ion polished. To prepare samples for polishing, the dactyl was embedded in epoxy (System 2000, Fiberglast, USA), sectioned with a diamond blade, and polished with silicon carbide sand paper such that the region of interest was exposed. Ion milling was then performed with a cross section polisher (JEOL IB-09010CP). This technique provides a view of the cross-section of pore canals not obtainable via abrasive polishing due to sample smearing and the filling in of pores. Ion polished sections were milled at 5kV for 8 h.

Detailed examination of mineral and organic architecture

To observe the structure of the underlying organic phase in the striated region of the stomatopod club, demineralization was performed on a sagittal section. Prior to

demineralization, a club was mounted in epoxy and polished in the sagittal plane with graded diamond abrasive solutions to a 50 nm grit size. The sample was then fixed for 1 hr in a 2.5% solution of glutaraldehyde in HEPES buffer. Demineralization was then performed for 30 minutes in a solution of 3% acetic acid and 2.5% glutaraldehyde in DI water. Following demineralization, the sample was rinsed 4 times in fresh DI water then serially dehydrated in ethanol, prior to sputter coating with platinum and palladium and observation with SEM (XL30-FEG, Philips, USA) at an accelerating voltage of 10 kV.

Additional samples were observed using TEM. To prepare thin sections a club was mounted in epoxy and polished in the transverse plane. 100 nm thin sections were milled perpendicular to the transverse face (in the sagittal plane) with a Focused Ion Beam (FIB, FEI Strate 235 Dual Beam) and imaged using TEM (Zeiss Libra) at 120 kV accelerating voltage.

Synchrotron X-ray data was collected at Beamline X13B at the National Synchrotron Light Source, Brookhaven National Laboratory, using 19 keV X-rays ($\lambda$ = 0.65 Å) and a beam spot focused to ca. 5 μm × 5 μm. Specimens consisting of dactyl clubs embedded in Epofix resin were sliced with a diamond saw to create 0.5 mm thick slices, which were then mounted onto the beamline sample holder in transmission geometry. Transmitted X-ray intensity was recorded using a photodiode detector fixed beyond the sample at the beam stop and normalized by incident intensity measured with an upstream ion chamber. Diffraction data were acquired with a Princeton Instruments CCD detector approximately 15 cm beyond the sample. Frames were not corrected for spatial distortions within the detector optical taper. Using a sintered corundum standard, the software package *Datasqueeze*, and a JCPDS data card for corundum, we calibrated detector pixel positions to *Q*-values.

The orientation of chitin fibers was measured using the techniques described by Paris and Muller [41], assuming that crystalline chitin grains exhibit fiber symmetry (a preferred c-axis but no preferred orientation within the plane normal to that axis), while the arrangement of the grains breaks this symmetry, with an angle μ between the fiber axis and a reference axis (the transmitted X-ray beam direction) that can vary from place to place within the sample. First, the (110) reflection of chitin was identified, and intensity vs. $Q$ plots as a function of detector azimuth χ were generated, integrated over a range of $Q$ which bounded this reflection ($Q$ = 1.3-1.4 Å$^{-1}$). As the fibers deviate from orthogonality with the beam, the location of their reflections on the detector do not remain separated by 180° in χ but have centroids displaced by an angle η. Diffracted peaks will obey:

$$\cos(\eta) = \tan(\theta)/\tan(\mu),$$

where θ is one-half the Bragg scattering angle. However, this equation can only useful for values of μ above a threshold.

Preparation of cross-sections

Transverse cross-sections of stomatopod clubs, at two locations within the dactyl, were prepared by mounting samples in epoxy (System 2000, Fiberglast, USA). Samples were sectioned to the planes of interest using a diamond blade, and polished with graded diamond abrasive solutions to a 50 nm grit size. After SEM analysis, the same samples were subjected to demineralization under 5% acetic acid for 10 minutes with no fixation.

Transverse sections of a praying mantis tibia were prepared using the same procedure. Demineralization was not performed on praying mantis sections.

Determination of volume percent mineral and organic

Thermogravimetric analysis was employed to determine the relative volumetric content of mineral and organic in the stomatopod dactyl. To prepare samples for testing, the exocuticle (impact region) was removed with abrasive grinding. Efforts were made to isolate the striated region, though some periodic region unavoidably remained. Samples were ground to a fine powder using a mortar and pestle, and heated at 5° C/min to 1200° C under a nitrogen purge. Weight percent measurements were used to isolate various components of the cuticle, using the method proposed by Bobelmann et al. [42] To convert to an estimated volume percent, the density of water was used, along with the density of amorphous calcium carbonate and crystalline alpha chitin.[43] Though it is acknowledged that ACC and crystalline chitin do not comprise the entire mineral and organic phases, respectively, the use of these values provides a first approximation, and reasonable estimate for the development of micro-mechanical models.

Nanoindentation

Nanoindentation maps were performed on polished cross-sections of dactyl clubs in both the transverse and coronal orientation. Indents were performed under ambient temperature using a nanomechanical testing system (TI 950 Triboindenter, Hysitron, USA). Cross-sections of were prepared by mounting samples in epoxy (System 2000, Fiberglast, USA), sectioning to the planes of interest using a diamond blade, and polishing with graded diamond abrasive solutions to a 50 nm grit size. With flat polished sections prepared, load controlled indents were performed to 500 and 1000 μm, using a Berkovich indenter tip. The load function consisted of a 5 second loading step, 2 second hold, and 5 second unloading step. Hardness and elastic modulus were calculated from the unloading curve of each indent using the Oliver and Pharr method.[44] Average values from indent grids are presented in Supplemental Table 1.

Modeling Methodology

The Dynamic Finite Element Analysis (DFEA) of an impact event between the dactyl club and a solid target discussed in Figure 4 was carried out using the finite element software Abaqus/Explicit following the same methodology employed in.[17] Our model considered the entire geometry of the dactyl, the propodus, and the target. Because the terminal two segments of the raptorial appendages can be approximated as a solid of revolution, we carried out a 2D axisymmetric analysis. The dactyl club has an average total length of ca. 5 mm and a radius of ca. 2 mm. The entire distance from the top of the club (impact region) to the end of the propodus is ca. 10 mm. These dimensions are representative of a typical adult sized specimen of Odontodactylus scyllarus (and similar to the one analyzed in this paper and used for other previous experimental work). The mechanical response of the material was modeled as isotropic linear elastic with different mechanical properties and mass densities. The material properties were provided from ref. 17. In addition, the water-filled cavities (containing the internal musculature) of the dactyl and propodus were simulated as an acoustic medium to properly account for the wave propagation in the fluid and its interaction with the rest of the club. The finite element mesh contains a total of 433,787 nodes and 429,987 elements. In these simulations, the target initially traveled at 20 m/s and impacts the dactyl club producing a compressive stress wave traveling through both the target and dactyl. Because we were interested in the impact event, we did not consider the effect of the water surrounding the dactyl club (although we do consider the water inside the central cavity, as it is very important for transmission of the stress waves). Due to the relatively low impedance of water, the boundary of the dactyl and propodus were modeled as free surfaces.

The 3D geometries shown in Figures 2A and 5 were scanned and built (Purdue BioScience Imaging Facility [5]). The stiffness of each section was calculated as:

$$K_{\eta\eta} = \int_A \Gamma \rho^2 dA$$

where $dA$ is a differential area of arbitrary shape, $\rho$ is the distance between principal inertia axis $\eta\eta$ to d$A$ and $\Gamma$ is the Young's Modulus for bending or Shear Modulus for the torsion.

The technique employed to estimate the drag coefficient ($C_d$) of the spearer spike and smasher dactly club was taken from.[6,47] In this case, the profiles of the appendages are directly compared with known profiles whose values of $C_d$ have already been reported. The comparison between shapes was done considering bidimensional potential flow, zero angle of attack for any shape, the same type of fluid, length scale and Reynolds region. For both cases (i.e., the spearer spike and smasher dactyl club), we considered a relative velocity between the appendage and the fluid of 20 m/s. The kinematic viscosity for water at 20°C is $1.003 \times 10^{-6} m^2/s$. The characteristic dimension for the spike "*d*" is defined as the length of the cross section (chord), which is 4.5 mm. The characteristic dimension for the smasher "*d*" is the length of the dactyl plus the propodus, which is between 1 - 2 cm. Using these values, the Reynolds number (Re) for the spike is approximately $\mathrm{Re} \approx 9 \times 10^4$ and for the smasher is $\mathrm{Re} \approx 4 \times 10^5$. Most of the equivalent profiles shown in Figures 5C and 5D are based on standard geometries. However, the geometry of the dactyl club and propodus system (shown at the bottom of Figure 5D), was approximated as a symmetric NACA airfoil, but with a maximum width of 40% of the chord and a maximum curvature of 20% at the leading edge. The hydrodynamic characteristic of this airfoil, in particular, was calculated using XFLR5 software from Mark Drela and Harold Youngren.[48]

An additional analysis was carried out to characterize the elastic properties of the striated region. The purpose of this analysis is to corroborate the values obtained with the characterization and nanoindentation work and to provide more insights into the hierarchical structure of the fibrous structure. As previously discussed, the striated region was found to consist of long fibers, assembled with a circular configuration that circumferentially wrap around the entire periodic region. Supplementary Figure S1 depicts an 18x18x18 μm 3D representative volume element (RVE) of the microstructure of the striated region showing the transverse (plane *xy*), sagittal (plane *yz*) and coronal sections (plane *zx*). In particular, we focus our modeling on the prediction of the elastic properties in the direction z and compare those with the nanoindentation performed on the transverse plane (see C in Supplemental Figure S1). The striated region presents a hierarchical structure with nanoscale $\alpha$-chitin / mineral fibrils assembling at the microscale to form highly aligned sheets of composite fibers (see Supplemental Figure S1).

Based on observations in similar species,[49,50] we assume the following three hierarchical levels for the striated region:

**Level I** (Figure S1-A): Fibrils are composed of crystalline *a*-chitin and amorphous $CaCO_3$ and $CaPO_4$. We surmise proteins are present as well.

**Level II** (Figure S1-B): The fibrils from I are bundled into fibers.

**Level III** (Figure S1-C): The fibers from II are arranged in sheets and embedded in a matrix of amorphous mineral. At this particular length scale, we observe that the fibers are parallel to the pore canals (also observed in Supplemental Figure 2).

Due to the uncertainties and lack of details of the actual structure below 100 nm, which includes the actual composition and geometry of the fibril and fiber structures described in levels I and II, we propose to focus our predictions on what is known at level III. As such, we adopt the material properties from the basic building blocks and measured values of volume fractions of organic and inorganic materials to calculate the basic elastic properties of the striated region. The geometry of level III is shown in Figure S1-C, where the main fibers are depicted in yellow and the mineral sheets in green. At this level, the mechanical properties of the mineral sheets are obtained from a combination of amorphous $CaCO_3$, $CaPO_4$ and protein. Thermogravimetric analysis (TGA) measurements reveal a water content of 22.26 vol%, an organic content of 15.6 vol% and a mineral content of 62.14 vol%. While the organic contents correspond to α-chitin and protein, the mineral content corresponds to ACC and ACP.

To calculate the effective Young Modulus of the matrix, we employed the method of Mori-Tanaka.[51] Because of the relative low stiffness of the proteins, their contribution to the overall elastic properties of the mineral matrix is neglected. Only the α-chitin is considered as the organic component. The Young's Modulus for the α-chitin is assumed to be 1 GPa.[52]

We then consider a 2D computational unit cell that represents the material observed from the sagittal face (Figure S1-C). The unit cell contains fibers surrounding the characteristic pore canals. The elastic properties of the fibers (yellow) are computed considering a mixture of amorphous mineral with a Young's Modulus of 32-37 GPa[49,50,53] and α-chitin. The thickness of each stack of fibers is 0.1 μm. The Young's modulus of the green region is 4 MPa. Periodic boundary conditions were applied to the model to ensure that the RVE actually represents an infinite material with a periodic pattern. Due to the fact that indentation was done on the transverse face of the material, fibers are mostly under compressive loads in our simulations.

Considering the uncertainties in the basic material properties and volume fractions of all the constituents, the resulting effective Young's modulus was 18.4 ± 1.6 GPa. These values were similar to our experimental results (ca. 17.6 GPa), confirming the validity of our simplified model.



**Supporting Information**

Supporting Information is available from the Wiley Online Library or from the author.

**Acknowledgements**

Miss Regina Campbell at JEOL is acknowledged for preparation of ion polished samples. This research was supported by a grant from the Air Force Office of Scientific Research (AFOSR-FA9550-12-1-0245) and the Air Force Office of Scientific Research, Multi-University Research Initiative (AFOSR-FA9550-15-1-0009). Dr. David Kisailus would like to acknowledge financial support from the AFOSR DURIP Grant FA9550-10-1-0322 for the nanoindenter. N.A. Yaraghi would like to acknowledge financial support from the National Defense Science and Engineering Graduate (NDSEG) fellowship.

Submitted to ADVANCED MATERIALS

Received: ((will be filled in by the editorial staff))

Revised: ((will be filled in by the editorial staff))

Published Online: ((will be filled in by the editorial staff))



**References**

1 Full, R., Caldwell, R. & Chow, S. Smashing energetics: Prey selection and feeding efficiency of the stomatopod, *Gonodactylus bredini*. *Ethology* **81**, 134-147 (1989).

2 Ahyong, S. T. Phylogenetic analysis of the Stomatopoda (Malacostraca). *Journal of Crustacean Biology* **17**, 695-715 (1997).

3 Currey, J., Nash, A. & Bonfield, W. Calcified cuticle in the stomatopod smashing limb. *Journal of Materials Science* **17**, 1939-1944 (1982).

4 Schram, F. Paleozoic proto-mantis shrimp revisited. *Journal of Paleontology* **81**, 895-916 (2007).

5 Jenner, R., Hof, C. & Schram, F. Palaeo- and achaeostomoatopods (Hoploccarida: Crusteacea) from the Bear Gulch Limestone, Mississippian (Namurian), of central Montana. *Contributions to Zoology* **67**, 155-186 (1998).

6 Haug, J., Haug, C., Maas, A., Kutschera, V. & Waloszek, D. Evolution of mantis shrimps (Stomatopoda, Malacostraca) in the light of new Mesozoic fossils. *BMC Evolutionary Biology* **10** (2010).

7 Schram, F. Paleosquilla gen. nov. - a stomatopod (Crustacea) from the Cretaceous of Columbia. *Journal of Paleontology* **42**, 1297-1301 (1968).

8 Föster, R. Heuschreckenkrebse (Crstacea, Stomatopoda) aus dem Alttertiär von Helmmstedt und Handorf (Niedersachsen) und der Oberkreide von Nigeria. *Neues Jahrbuch für Geologie und Paläontologie Abhandlungen M.H.* **6**, 321-335 (1982).

9 Ahyong, S. & Harling, C. The phylogeny of stomatopod Crustacea. *Australian Journal of Zoology* **48**, 607-642 (2000).

10 Porter, M., Zhang, Y.-F., Desai, S., Caldwell, R. & Cronin, T. Evolution of anatomical and physiological specialization in the compound eyes of stomatopod crustaceans. *Journal of Experimental Biology* **213**, 3473-3486 (2010).

11 Vermeij, G. *Evolution and Escalation*. (Princeton University Press, 1987).

12 Harper, E. *Predator-Prey Interactions in the Fossil Record*. (Kluwet Academic/Plenum Publishers, 2003).

13 Geary, D., Allmon, W. & Reaka-Kudla, M. Stomatpod predation on fossil gastropods from the Plio-Plesitocene of Florida. *Journal of Paleontology* **65**, 355-360 (1991).

14 Baluk, W. & Radwanski, A. Stomatopod predation upon gastropods from the Kortynica Basin and from other classical Miocene localities in Europe. *Acta Palaeoneontological Polonica* **46**, 279-304 (1996).

15 Patek, S., Korff, W. & Caldwell, R. Deadly strike mechanism of a mantis shrimp. *Nature* **428**, 819-820 (2004).

16 deVries, M., Murphy, E. & Patek, S. Strike mechanics of an ambush preditor: the spearing mantis shrimp. *Journal of Experimental Biology* **215**, 4374-4384 (2012).

17 Weaver, J. *et al.* The stomatopod dactyl club: A formidable damage-tolerant biological hammer. *Science* **336**, 1275-1280 (2012).

18 Bouligand, Y. Twisted fibrous arrangements in biological materials and cholesteric mesophases. *Tissue & Cell* **4**, 189-217 (1972).

19 Grunenfelder, L. K., Herrera, S. & Kisailus, D. Crustacean-derived biomimetic components and nanostructured composites. *Small*, doi:10.1002/smll.201400559 (2014).

20 Kaw, A. K. *Mechanics of Composite Materials*. Second edn, (CRC Press, 2006).

21 Fabritius, H.-O., Sachs, C., Triguero, P. R. & Rabbe, D. Influence of structural principles on the mechanics of a biological fiber-based composite material with hierarchial organization: The exoskeleton of the lobster *Homarus americanus*. *Advanced Materials* **21**, 391-400 (2009).

22 Romano, P., Fabritius, H. & Rabbe, D. The exoskeleton of the lobster Homarus americanus as an example of a smart anisotropic biological material. *Acta Biomaterialia* **3**, 301-309 (2007).

23 *Biology of the lobster homarus americanus*. (Acadmic Press, 1995).

24 Fabritius, H.-O. *et al.* Correlation of structure, composition and local mechanical properties in the dorsal carpace of the edible crab *Cancer pagurus*. *Crystalline Materials* **227**, 766-776 (2012).

25 Hegdahl, T., Gustavsen, F. & Silness, J. The structure and mineralization of the carapace of the crab (*Cancer pagurus* L.) 3. The epicuticle. *Zoologica Scripta* **6**, 215-220 (1977).

26 Neville, A., Thomas, M. & Zelanzy, B. Pore canal shape related to molecular architecture of arthropod cuticle. *Tissue & Cell* **1**, 183-200 (1969).

27 Patek, S. & Caldwell, R. Exterme impact and cavitation forces of a biological hammer: strike forces of the peacock mantis shrimp *Odontodactylus scyllarus*. *The Journal of Experimental Biology* **208**, 3655-3664 (2005).

28 Shih, C. Relationships between the J-integral and the crack opening displacement for stationary and extending cracks. *J. Mech. Phys. Solids* **29**, 305-326 (1981).

29 Wise, J. & Grady, J. in *Proceedings of High Pressure Science and Technology, APS Meeting.* (eds SC Schmidt, JW Shaner, GA Samara, & M Ross) 777.

30 Espinosa, H., Zavattieri, P. & Emore, G. Adaptive FEM Computation of geometric and material nonlinearities with application to brittle failure. *special issue of Mechanics of Materials* **29**, 275-305 (1998).

31 Shockey, D. *et al.* Failure phenomenology of confined ceramics targets and impacting rods. *Int. J. of Impact Eng* **9**, 263-275 (1990).

32 Salom, P. R., Gergely, J. & Young, D. T. Torsional strengthening of spandrel beams with fiber-reinforced polymer laminates. *Journal of Composites for Construction* **8**, 157-162 (2004).

33 Shan, L. & Qiao, P. Flexural-torsional buckling of fiber-reinfored plastic composite open channel beams. *Composite Structures* **68**, 211-224 (2005).

34 Claverie, T., Chan, E. & Patek, S. N. Modularity and scaling in fast movements: Power amplification in mantis shrimp. *Evolution* **65**, 443-461 (2011).

35 Claverie, T. & Patek, S. Modularity and rates of evolutionary change in a power-amplified prey capture system. *Evolution* **67**, 3191-3207 (2013).

36 Patek, S., Rosario, M. & Taylor, J. Comparative spring mechanics in mantis shrimp. *The Journal of Experimental Biology* **216**, 1317-1329 (2013).

37 Zack, T., Claverie, T. & Patek, S. Elastic energy storage in the mantis shrimp's fast predatory strike. *The Journal of Experimental Biology* **212**, 4002-4009 (2009).

38 Fabritius, H. *et al. Chitin in the exoskeletons of arthropoda: from ancient design to novel materials science*. (Springer, 2011).

39 Batchelor, G. *An Introduction to Fluid Dynamics*. (Cambridge University Press, 1967).

40 Patek, S., Nowroozi, B., Baio, J., Caldwell, R. & Summers, A. Linkage mechanics and power amplification of the mantis shrimp's strike. *The Journal of Experimental Biology* **210**, 3677-3688 (2007).

41 Paris, O. & Muller, M. Scanning X-ray microdiffraction of complex materials: Diffraction geometry considerations. *Nuclear Instruments and Methods in Physics Research Section B: Beam Interactions with Materials and Atoms* **200**, 390-396 (2003).

42 Bobelmann, F., Romano, P., Fabritius, H., Rabbe, D. & Epple, M. The composition of the exoskeleton of two crustacea: The American lobster *Homarus americanus* and the edible crab *Cancer pagurus*. *Thermochemica Acta* **463**, 65-68 (2007).

43 Raabe, D., Al-Sawalmih, A., Yi, S. & Fabritius, H. Preferred crystallographic texture of a-chitin as a microscopic and macroscopic design principle of the exoskeleton of the lobster *Homarus americanus*. *Acta Biomaterialia* **3**, 882-895 (2007).

44 Oliver, W. & Pharr, G. Measurement of hardness and elastic modulus by instrumented indentation: Advances in understanding and refinements to methodology. *Journal of Materials Research* **19**, 3-20 (2004).

45 *http://www.purdue.edu/discoverypark/bioscience/facilities/imaging/*.

46 Hoerner, S. F. *Fluid Dynamic Drag: Practical Information on Aerodynamic Drag and Hydrodynamic Resistance*. 2 edn, (Hoerner Fluid Dynamics, 1965).

47 White, F. M. *Fluid Mechanics*. 4th edn, (McGraw Hill, 2001).

48 *http://www.xflr5.com*.

49 Nikolov, S. *et al.* Robustness and optimal use of design principles of arthropod exoskeletons studied by ab initio-based multiscale simulations. *Journal of the Mechanical Behavior of Biomedical Materials* **4**, 129-145 (2011).

50 Nikolov, S. *et al.* Revealing the design principles of high-performance biological composites using Ab initio and multiscale simulations: The example of lobster cuticle. *Advanced Materials* **22**, 519-526 (2010).

51 Mori, T. & Tanaka, K. Average stress in matrix and average elastic energy of materials with misfitting inclusions. *Acta Metalurgica* **21**, 571-574 (1973).

52 Nair, K. G. & Dufresne, A. Crab Shell Chitin Whisker Reinforced Natural Rubber Nanocomposites. Mechanical Behavior. *Biomacromolecules* **4**, 657-665 (2003).

53 Fan, Y., Sun, Z., Wang, R., Abbott, C. & Moradian-Oldak, J. Enamel inspired nanocomposite fabrication through amelogenin supramolecular assembly. *Biomaterials* **28**, 3034-3042 (2007).

54 Ehrlich, H. et al. Supercontinuum generation in natrually occuring glass sponge spicules. *Advanced Optical Materials* **4**, 1608-1613 (2016).

55 Birchall, J.D., Thomas, N.L. On the architecture and function of cuttlefish bone. *Journal of Materials Science* 18, 2081-2086 (1983)



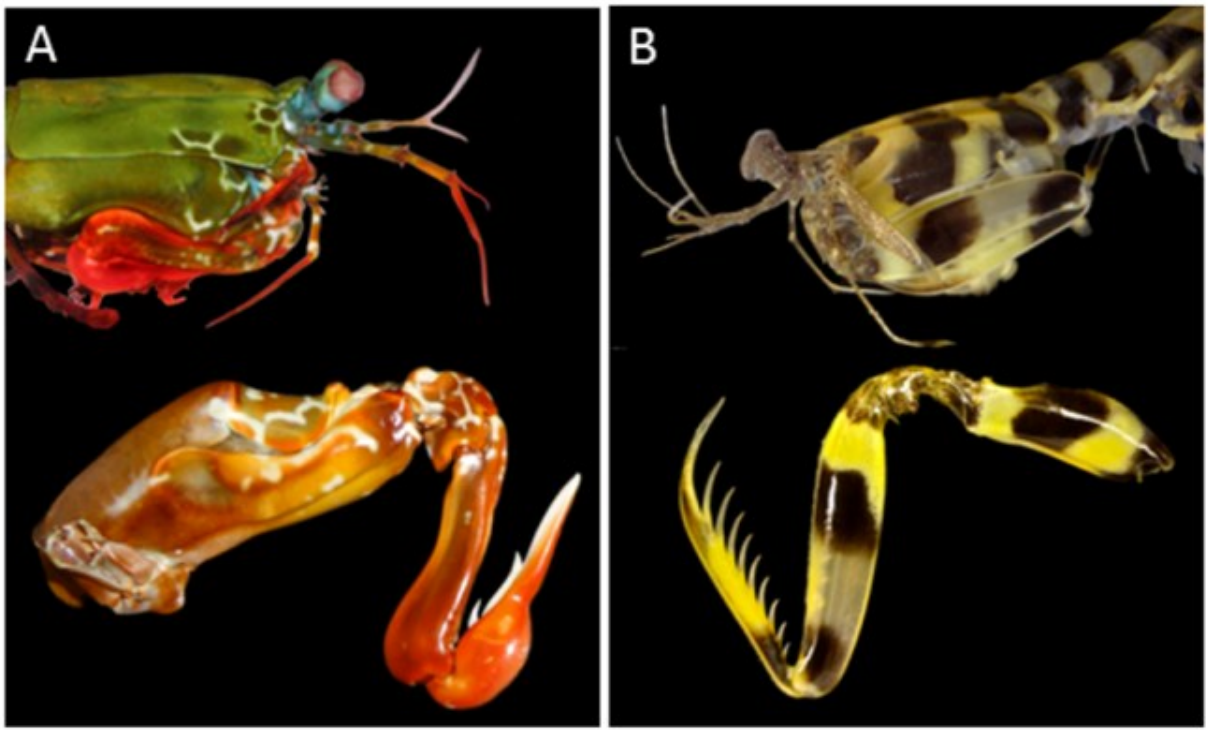


**Figure 1:** Stomatopods are divided into two groups based on the structure of their feeding appendage. The structure of the dactyl from the second maxilliped enables the identification of (A) a bulbous hammer from the smasher *Odontodactylus scyllarus* and (B) a harpoon-like raptorial appendage from the spearer *Lysiosquillina maculate*.

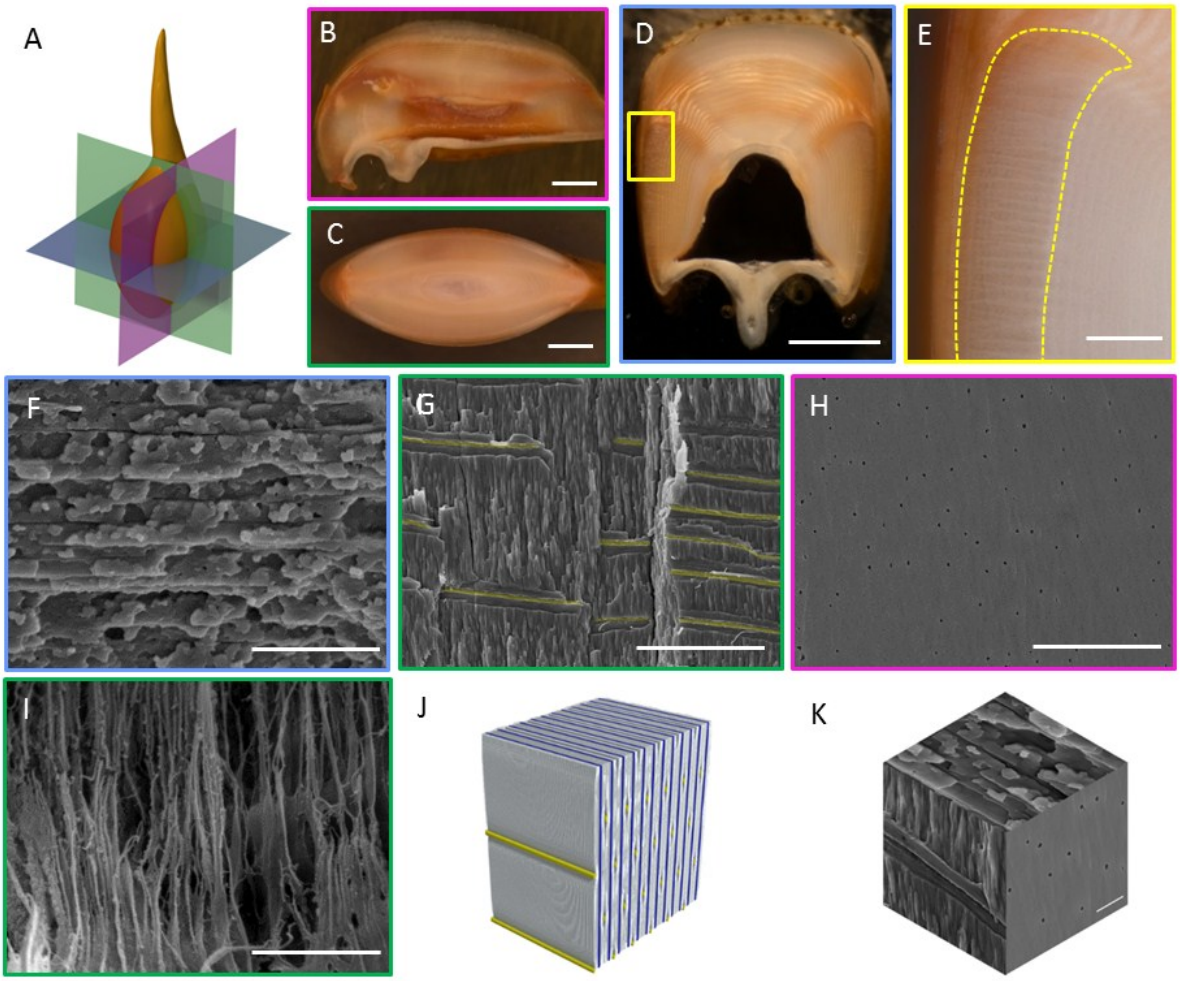


**Figure 2:** A clarified structure of the striated region viewed in three perpendicular directions. The planes of view are the (A) sagittal (magenta, B), coronal (green, C) and transverse (blue, D). Scale bars in (B)-(D) are 1mm. The striated region is observed on each side of a transverse cross-section and is defined by a series of parallel striations (E). Scale bar in (E) is 200 µm. SEM micrographs of fractured specimens reveal stacked sheets of parallel fiber layers in a transverse section (F), and a side view of pore canals (highlighted in yellow) connected by perpendicular mineralized fiber layers in a coronal section (I). A network of pore canals is clear in an ion polished (H) sagittal section, Scale bars in (F) – (H) are 10 µm. Demineralization of a sagittal section (I) reveals a predominately bundled architecture of the organic □-chitin, and the parallel fiber structure. Scale bar in (I) is 2 µm. A schematic showing the architecture of the striated region is presented in (J), and a three-plane representation with SEM micrographs is shown in (K). Scale bar in (K) is 2 µm.

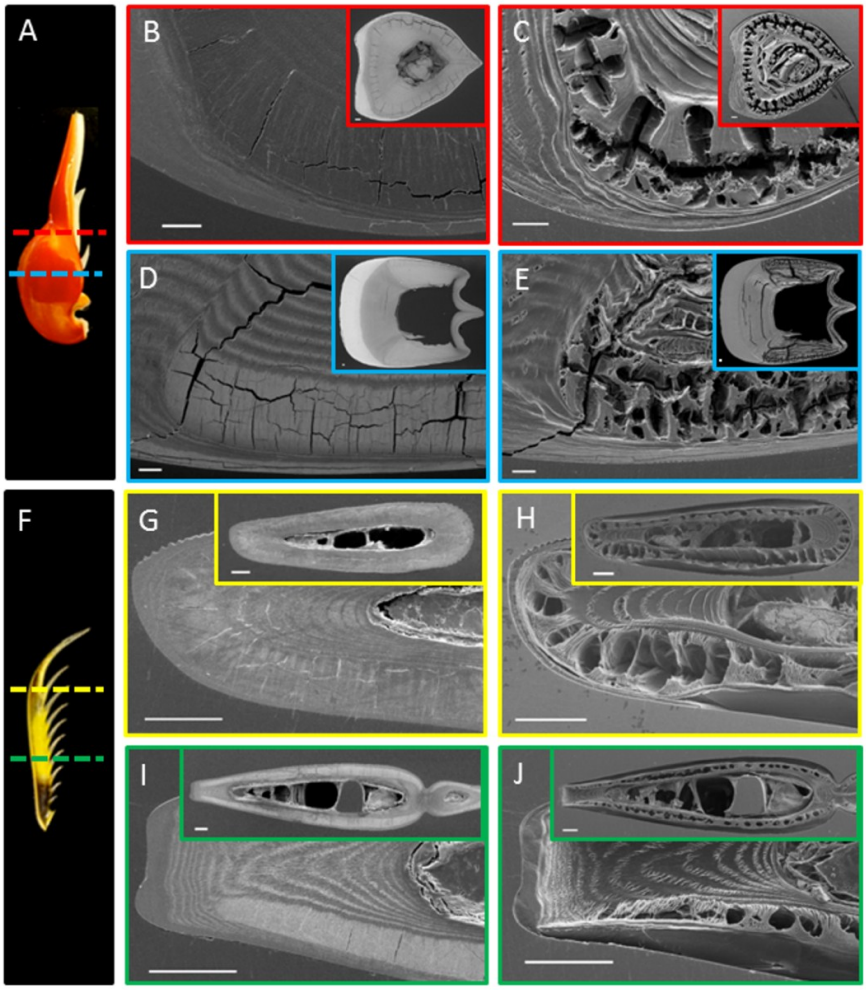


**Figure 3:** The striated region has been repurposed in the impact zone of the smasher club to provide impact resistance. (A) Bulk view of smasher club, with dashed lines showing the locations of cross sections at the center of the club (blue) and the base of the spike (red). SEM micrographs at the base of the spike before (B) and after (C) demineralization, revealing the striated region, which wraps the entire structure. Micrographs in the impact zone of the bulb of the club before (D) and after (E) demineralization revealing a striated region isolated on either side of the club. (F) Bulk view of a spearer spike, with dashed lines highlighting the locations of cross sections at the center (green) and tip (yellow) of the spear. SEM micrographs near the top of the spike before (G) and after (H) demineralization demonstrating a striated region that wraps the entire structure. Micrographs at the center of the spike before (I) and after (J) demineralization, showing that the striated region wraps the entire club at all locations, providing evidence for impact tolerant exaptation in the smasher club structure.

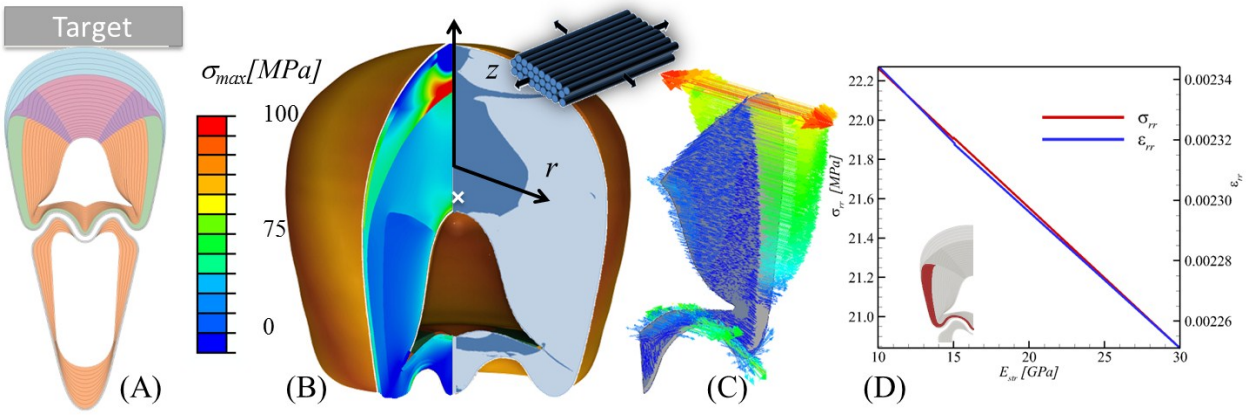


**Figure 4:** Schematics of the dynamic finite element analysis (DFEA) of a dactyl club/propodus system striking a flat target at 20 m/s. (B) Transverse section showing the maximum principal stress $\sigma_{max}$ at ~2 ms after impact (left side) and biaxial stress map indicating those regions where $\sigma_r \approx \sigma_\theta > 0$ (right) with dark blue. (C) Principal directions acting on a radial plane of the dactyl club, showing that the principal directions are parallel to the fibers in the striated region. The inset shows the striated region in red (D) Peak value of the radial stress and strain in the center of the dactyl club (indicated by an "x" in (B)) for various values of the Young's Modulus in the striated region ($E_{str}$), highlighting the role of confinement.

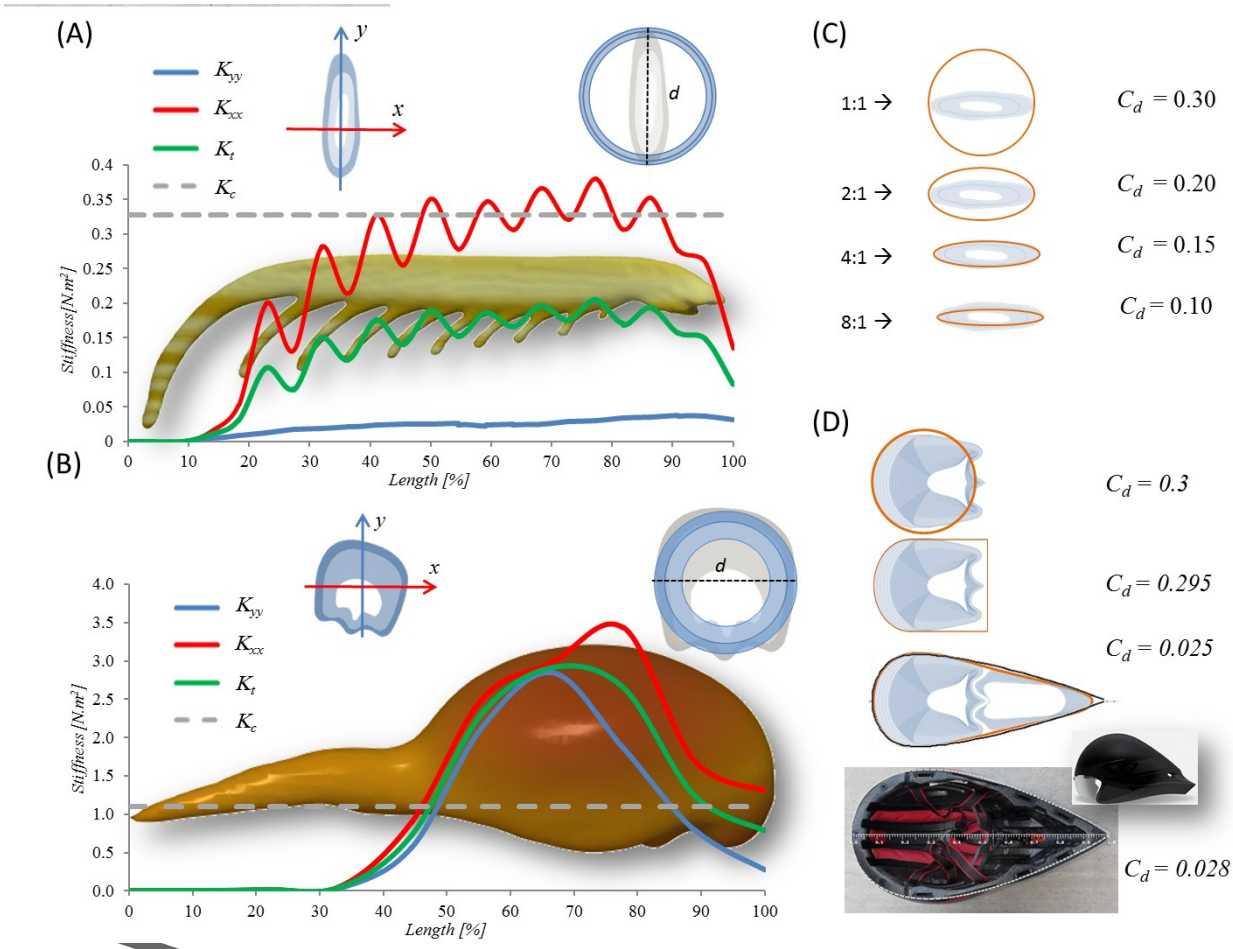


**Figure 5:** Variation of the bending stiffness', $K_{xx}$ and $K_{yy}$, and torsional stiffness, $K_t$, along the longitudinal axis of the spearer spike (A) and smasher dactyl club (B). The principal directions, *x* and *y*, are denoted for both cases in the inset figure on the left. The inset figure on the right presents a comparison of the cross section with an equivalent circular cross sectional tube with the same diameter ($d$) and average area of the spear cross section. Drag coefficient of different airfoil and shape profiles compared with the spearer spike (C) and smasher dactyl club (D) for a turbulent regime ($Re > 10^4$). The $C_d$ for an aerodynamic helmet, which has a strikingly similar profile as the combined dactyl and propodus, is included for comparison purposes.

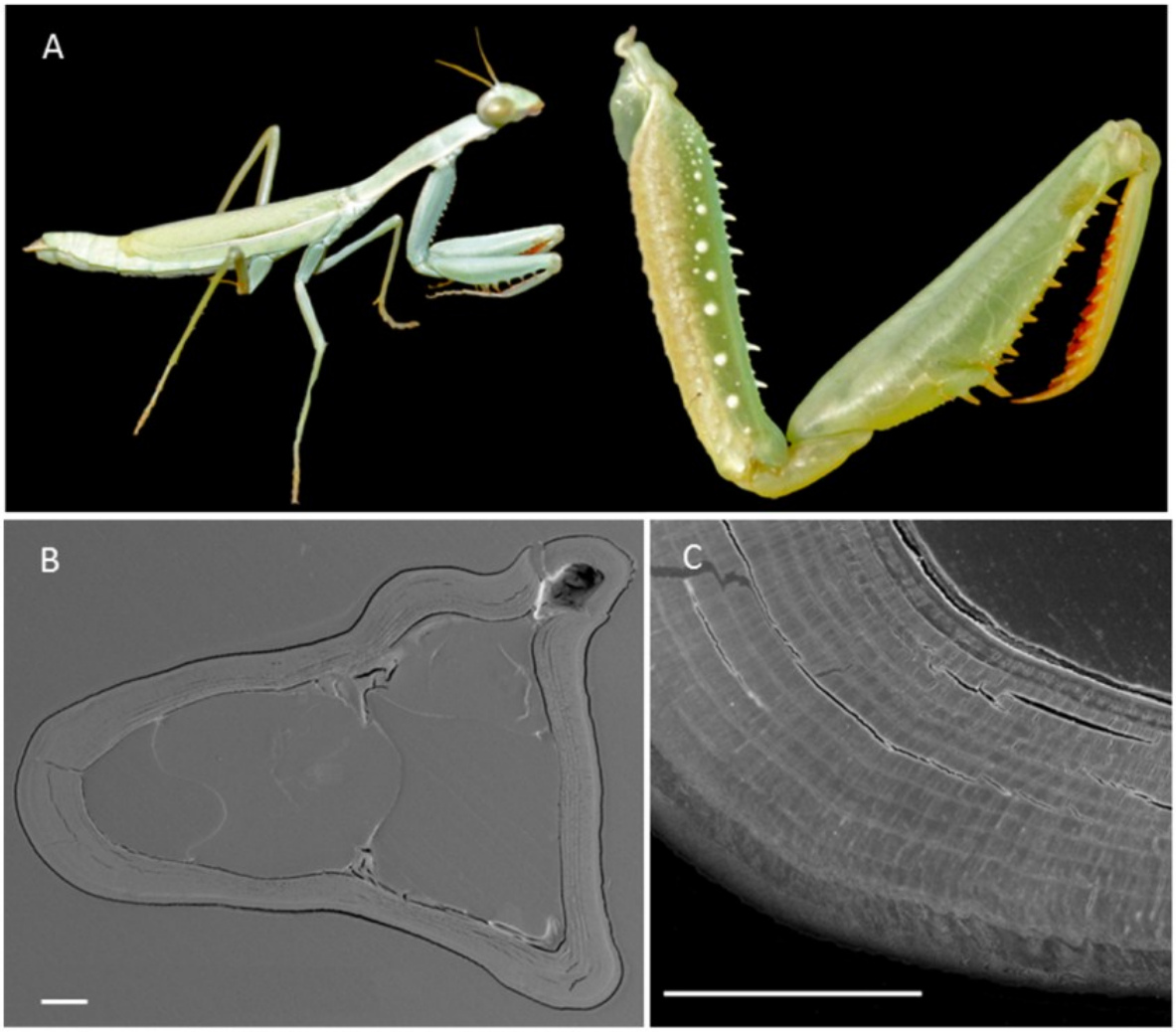


**Figure 6:** (A) Photograph of the praying mantis, *Stagmomantis limbata*, highlighting the raptorial appendage of the organism. (B) Transverse cross-section of the tibia (C) Magnified view of tibia, showcasing the lack of a striated region. Scale bars in B and C are 100 μm.

**Table of Contents**

A highly aligned and mineralized structure is identified within the exocuticle of an impact-resistant crustacean appendage. This regional composite structure features circumferentially wrapped unidirectional chitinous fibers consisting of amorphous calcium carbonate and calcium phosphate that place the club under compression during high-energy strikes. We also reveal macro-morphological hydrodynamic features that significantly reduce drag, which enables the stomatopods to accelerate to strike at incredibly high rates.

Keywords: (Composites, Toughness, Impact, Biomineral, Ultrastructure)

L.K. Grunenfelder, G. Milliron, S. Herrera, I. Gallana, N. Yaraghi, N.C. Hughes, K. Evans-Ludderodt, P. Zavattieri, D. Kisailus

**Ecologically driven ultrastructural and hydrodynamic designs in stomatopod cuticles**